Journal of Alloys and Compounds 501 (2010) 221–226

Contents lists available at ScienceDirect

Journal of Alloys and Compounds

journal homepage: www.elsevier.com/locate/jallcom

The interaction of Zr_2Fe surface with O_2 and H_2O at the temperature range 300–770 K

Shimon Zalkind, Moshe Nahmani, Noah Shamir*

Nuclear Research Centre – Negev, P.O. Box 9001, Beer-Sheva 84190, Israel

ARTICLE INFO

Article history:
Received 23 November 2009
Received in revised form 22 January 2010
Accepted 28 January 2010
Available online 23 March 2010

Keywords:
Getter
Oxidation
Degradation
Oxygen
Water vapor

ABSTRACT

The surface of metallic Zr_2Fe was exposed to oxygen and water vapor, in order to study the effects of these gases, being the main degradation agents in its operation as a getter for hydrogen. It was found that both gases oxidize the Zr component of the alloy surface, leaving the Fe metallic and strongly diluted. The oxidation is temperature and pressure dependent and under oxygen pressure of up to 5×10^{-6} Torr the oxide thickness increases with temperature up to ~470 K. At higher temperatures, above 570 K, the oxide film growth becomes predominated by decomposition and diffusion of oxygen into the substrate and higher oxygen pressure is needed to compensate the oxygen dissolution. It was found that for oxygen pressure of 1×10^{-5} Torr and 620 K, which is the operating temperature of the getter, the oxidation is most effective, since both the adsorption and inward diffusion are efficient. The oxide film thickness, at these conditions, is about the XPS probing depth (~5 nm). For 770 K, the dissolution and inward diffusion are very fast and the adsorption not efficient enough, leaving a dissolved and depleted oxygen layer at the surface. The initial sticking coefficients per oxygen atom, at RT, are similar for oxygen and water vapor, but the oxide thickness, obtained for H_2O, is more than twice of that for O_2, which points to a different oxidation mechanism. The presence of oxygen vacancies or incorporation of hydroxyl groups in the oxide layer may be the factors enabling further inward growth.

1. Introduction

The Zr_2Fe alloy belongs to the non-evaporable getters (NEG) family. NEG materials have long been used in the industry for a variety of applications, which need maintaining of ultra-high-vacuum (UHV) such as high energy particle accelerators [1–3]. The most common NEG materials are metals, such as Zr, Ti, Nb, Ta, V that have a wide solubility range towards oxygen or hydrogen and alloys based on those metals. The NEG are usually easy to apply and manufacture as powder, pellets, thin layers, etc. [1–3]. Zr_2Fe was found to be effective in scavenging hydrogen down to very low concentrations and can be used, for example, to prevent the release of tritiated heavy water [4] or for fuel purification in a fusion fuel cycle [5]. It is used for a variety of applications, like gas purification from hydrogen and its isotopes [6–9], hydrogen storage [10], safeguarding of hydrogen high pressure vessels and hydrogen retrieval from several gas mixtures [6]. It has been found that this alloy can absorb hydrogen up to 46% of its volume. It can also selectively absorb hydrogen from an N–H mixture, efficiently and selectively, up to 720 K, without disintegration [11]. This absorption forms two phases (disproportionation), ZrH_2 and $ZrFe_2$ [4,12]. Surface poisoning due to pre-exposure to gases like oxygen, water vapor, CO_2 and methane can reduce or even prevent hydrogen absorption [14].

The temperature effect on the surface composition of Zr_2Fe was studied by XPS [7,13,14]. It was found that heating the alloy to 470–1070 K causes a decrease of the spectral lines of oxygen contained components and an increase of the metallic ones. The atomic concentration of surface zirconium is increased to 75%, compared to the 66%, which is the nominal bulk value, on the expense of surface Fe due to surface segregation of Zr. The oxidation by oxygen was also studied by XPS and AES [15,16] at room temperature (RT), finding that sub-stochiometric oxides are formed on the surface.

The aim of the present study is to specify and understand the degradation mechanism of the getter, by oxygen and water vapor contaminations, in the temperature range 300–770 K.

2. Experimental

The study was performed in a UHV system (~2×10^{-10} Torr baseline pressure), which has been described in detail in previous publications (e.g. [17]), utilizing direct recoils spectrometry (DRS), Auger electron spectroscopy (AES) and X-ray photoelectron spectroscopy (XPS).

The DRS is based on grazing irradiation of the surface with a pulsed beam of 3 keV Ar^+ ions, and the time of flight measurements of the surface atoms (and ions) which are recoiled in a forward direction, following the direct collision inflicted by the impinging primary ions. The main characteristics of this technique are topmost surface sensitivity, detection of light atomic masses, including hydrogen, and being

* Corresponding author. Tel.: +972 8 6568785; fax: +972 8 6568751.
E-mail address: noah.shamir@gmail.com (N. Shamir).

0925-8388/$ – see front matter © 2010 Elsevier B.V. All rights reserved.
doi:10.1016/j.jallcom.2010.01.165

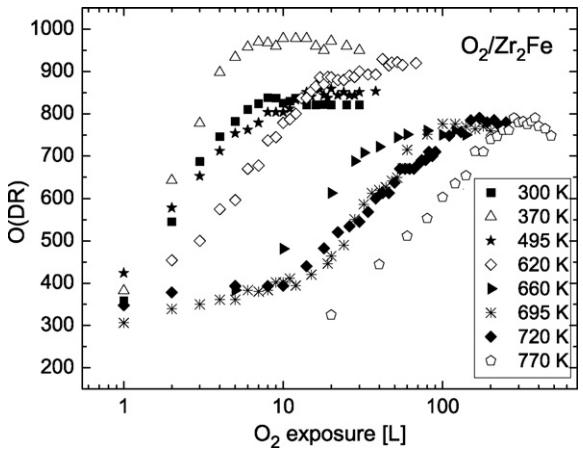

Fig. 1. O(DR) vs. exposure to oxygen (in Langmuirs) of Zr_2Fe, for various temperatures.

non-destructive, due to the low dose of impinging ions, needed for a good quality spectrum [18–20]. The combination of DRS and electron spectroscopy methods (e.g. AES, XPS) which probe to a deeper range beneath the surface, may resolve between processes occurring at the topmost atomic layer and in the subsurface region. Shadowing or non-shadowing of surface residing hydrogen atoms, make DRS an especially effective method for the differentiation between partial and full dissociation of water molecules on the surface [21,22].

The Zr_2Fe sample was gradually polished down to 1 μm by diamond paste, cleaned in distilled water and ethanol and then attached by spot-welding to two Ta wires, which enabled heating by driving an electric current through them. The sample temperature was monitored by a Chromel–Alumel thermocouple, spot welded to the sample edge. Sputter-cleaning was performed, before each exposure experiment, by a 5 kV Ar^+ ion beam during heating the sample to ~770 K and then lowering the temperature (during sputtering) to the desired one, in order to achieve maximum cleanliness of the surface and to avoid possible preferential sputtering.

3 keV electrons were used for the AES measurements and a Mg (E = 1253.6 eV) anode for the XPS measurements. For Zr(3d), λ ~ 2 nm, so the XPS depth sensitivity is ~5 nm.

3. Results

3.1. O_2/Zr_2Fe

Fig. 1 presents the O(DR) intensity vs. O_2 exposure dose (in logarithmic scale) for various temperatures, between 300 and 770 K. Two groups of adsorption curves can be observed. The first one, for the low temperature range, between 300 and 620 K, has a higher growth rate with exposure and reaches higher saturation values than the other group 660–770 K. The abrupt decrease in oxygen accumulation rate and saturation value that can be observed in the narrow range 620–660 K, will be discussed in the next section. It should also be noted that in the low temperature range, the 370 K curve, rather than that of the lowest temperature, 300 K, has the highest growth rate and saturation intensity.

Fig. 2 presents some of the RT AES spectra (Zr and Fe range) measured after steps of exposure to O_2 at pressure range of 5×10^{-7} to 5×10^{-6} Torr. The decrease of the Fe intensity and energy shift of the Zr lines, turning from metallic to oxidic, are noticeable (Zr spectrum similar to that of clean and oxidized Zr metal [23]). Peak-to-peak intensities were served for AES quantifications of oxygen and Fe. The clean and oxidized Zr components were extracted from the spectra by linear regression assuming that the measured AES zirconium spectrum is composed of a linear combination of a clean and a fully oxidized Zr signals. Fig. 3 presents the RT relative change of intensities of metallic and oxidic Zr (Zr(m) and Zr(ox), respectively), Fe and oxygen vs. oxygen exposure dose. Zr and Fe were normalized to 1 for the clean surface and oxygen to the saturation value. It is clear that Fe is depleted on the surface during oxidation (of Zr), while the sum of Zr(m) and Zr(ox) is about constant. The AES

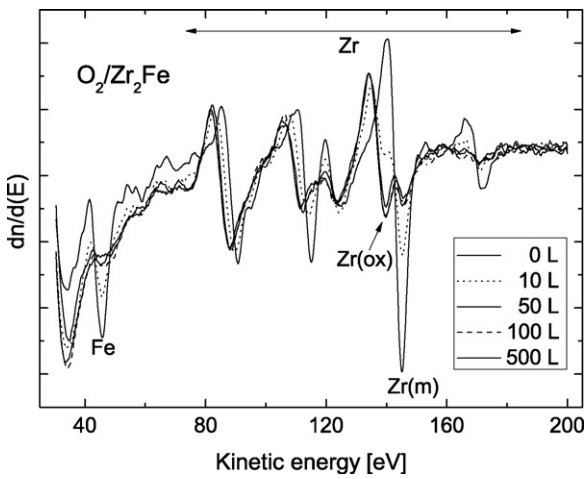

Fig. 2. Room temperature AES spectra of Zr_2Fe, clean (0 L) and exposed to various doses of oxygen. The Fe line and the metal (Zr(m)) and oxide (Zr(ox)) lines of Zr, are denoted. The arrow indicates the range used for oxide thickness calculations (Fig. 13).

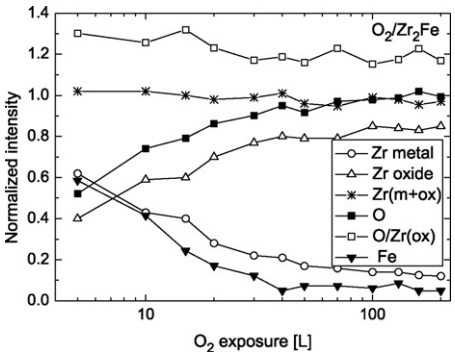

Fig. 3. Normalized (as indicated in the text) AES intensities of the Zr, Fe and O lines and also O/Zr(ox) vs. oxygen exposure dose, For RT exposures.

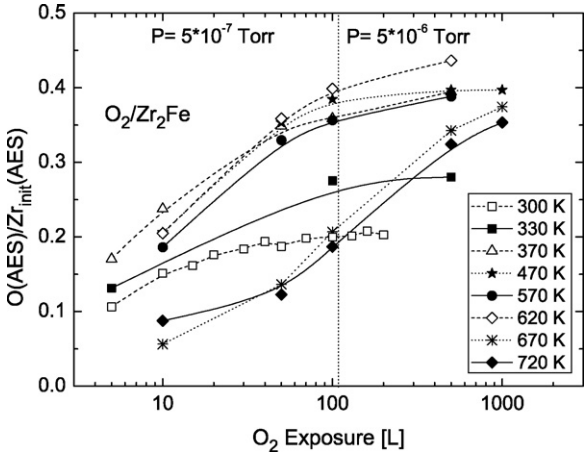

Fig. 4. O(AES) intensity (normalized to the clean Zr line) vs. exposure to oxygen, at various temperatures. The pressure of oxygen at each exposure range is indicated. The pressure of the 300 K exposure was 10^{-7} Torr.

intensity of oxygen, presented in Fig. 4 vs. exposure to oxygen, for some temperatures, presents a generally similar behavior to that of the O(DR) one (Fig. 1). The differences (that are significant) are discussed in the next section.

XPS measurements of the Zr(3d) binding energies for exposure to 1000 L O_2 at 1×10^{-5} Torr for 3 temperatures (Fig. 5), exhibit

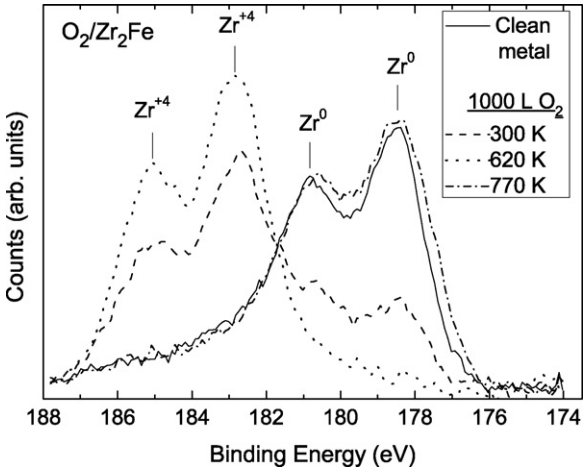

Fig. 5. Zr(3d) XPS spectra for clean Zr_2Fe and for exposure to 1000 L oxygen at $P = 10^{-5}$ Torr and various temperatures. The metallic Zr as well as Zr^{+4} (of ZrO_2) lines are indicated.

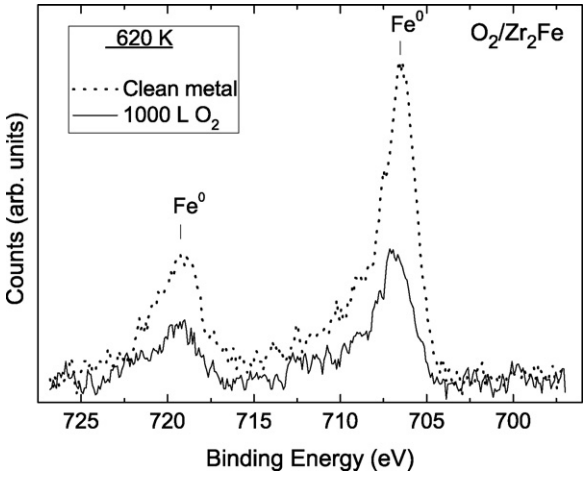

Fig. 6. Fe(2p) XPS spectra for 620 K, clean and 1000 L ($P = 10^{-5}$ Torr), exposed to oxygen Zr_2Fe. The energies of the metallic Fe are denoted.

full oxidation of the Zr component of the alloy, for the 620 K exposure and only partial oxidation for the lower as well as higher temperatures. The Fe(2p) component for all 3 temperatures (only 620 K presented, Fig. 6), does not exhibit any oxidation, in accordance with the Fe(AES) line. A clear decrease in the Fe(2p) intensity is observed, again, in accordance with the AES results. A single (oxidic) peak is observed for the O 1s excitation (not presented) and the maximum intensity is observed at 620 K, decreasing for 770 K.

In order to check the stability of the oxide with temperature increase, the Zr_2Fe sample was exposed to 1000 L O_2 at 310 K and then heated in steps while monitoring the O(KLL) AES intensity. Fig. 7 presents the oxygen intensity vs. temperature, exhibiting a fairly constant value up to ~570 K and then a decrease occurs, which is accelerated above 670 K.

3.2. H_2O/Zr_2Fe

Fig. 8 presents: (a) O(DR) vs. exposure for 300–770 K and (b) H(DR) vs. exposure for 300–620 K. For 620 K (as well as 770 K, not shown) the hydrogen intensity is practically zero. It can be observed that while for the 300–470 K range, the exposure dependence of O(DR) is quite similar (except for a slight decrease in saturation value), for 620 K the growth rate with saturation decreases significantly and for 770 K only a slight increase in the O intensity was detected.

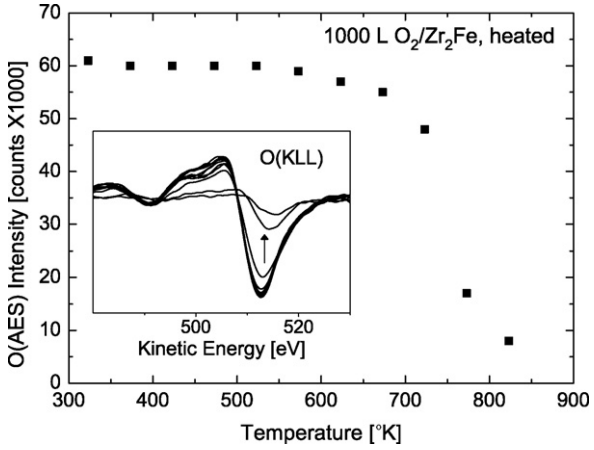

Fig. 7. O(KLL) intensity of Zr_2Fe, exposed to1000 L O_2 at RT, heated successively to temperatures as indicated in the figure. Inset: the O(KLL) line for the various temperatures.

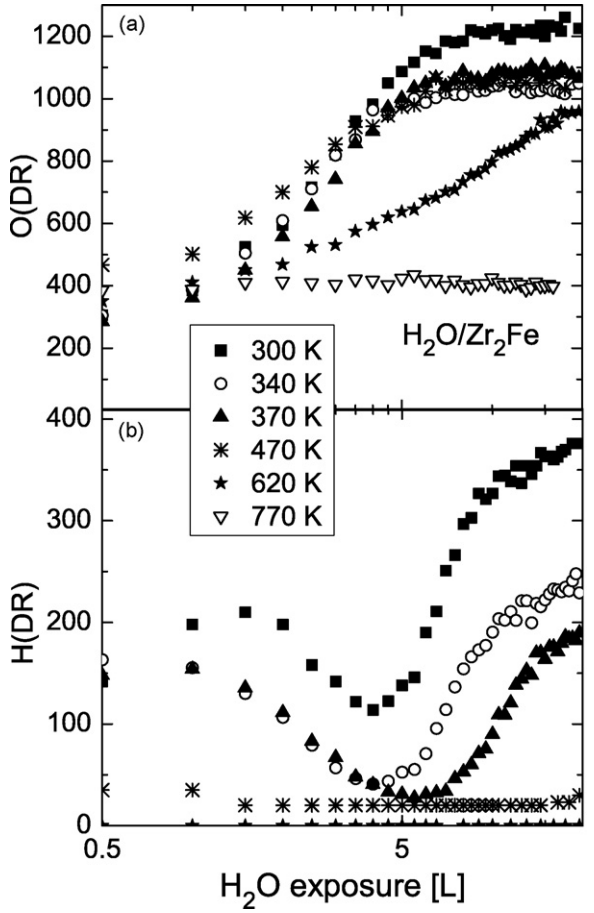

Fig. 8. (a) O(DR) and (b) H(DR) vs. exposure to H_2O of Zr_2Fe for various temperatures.

Fig. 9 presents the RT relative change of intensities of Zr(metallic + oxidic), Fe and oxygen (Zr and Fe normalized to 1 for the clean surface and oxygen to the saturation value) vs. H_2O exposure dose. As for the oxygen exposure, it is clear that Zr strongly segregates to the surface, driven by its oxidation, depleting the Fe by about 90%. Zr(m + ox), which is about constant for the O_2 exposure, decreases by about 20% for the initial H_2O exposure and then levels back to the initial value.

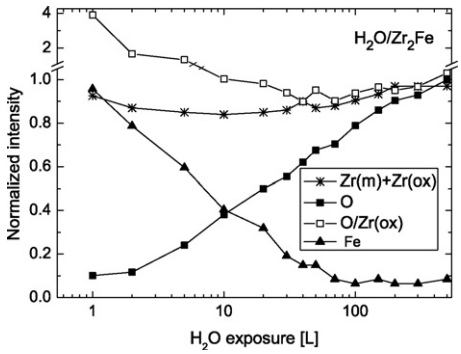

Fig. 9. Normalized (as indicated in the text) AES intensities of the Zr, Fe and O lines and also O/Zr(ox) vs. H_2O exposure dose, at RT.

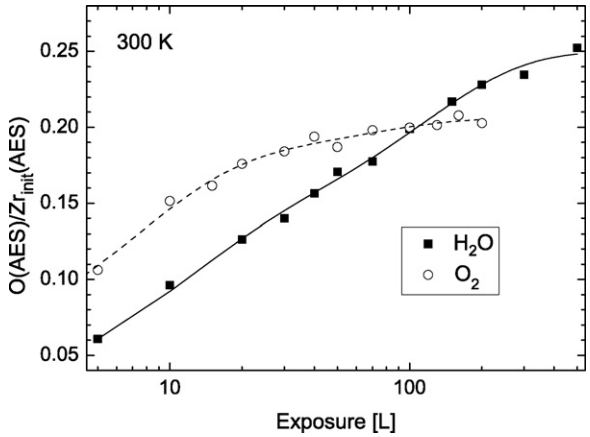

Fig. 10. Room temperature O(AES) intensity (normalized to the clean Zr line) vs. exposure to oxygen and H_2O.

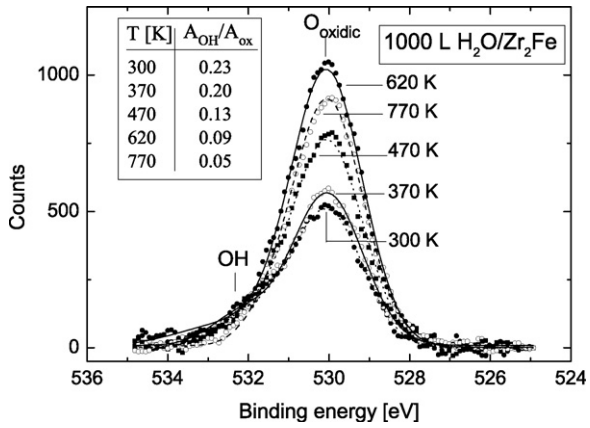

Fig. 11. XPS O 1s peak for 1000 L H_2O exposure, at various temperatures, together with the (calculated from two Gaussian fit) ratio of OH to oxidic peak intensities for each temperature.

The RT O(AES) intensity, normalized to that of clean Zr(AES), vs. exposure to H_2O, together with the O_2 exposure curve, for comparison, are presented in Fig. 10. While the initial increase of O(AES) for water vapor is slower than that for O_2 (as expected for half the O atoms), it continues to increase far beyond the asymptotic saturation of the O_2 adsorption curve. The differences between the two oxidation processes are discussed in the next section. XPS measurements of an adsorption sequence (5–250 L H_2O, not presented) yielded a clear oxidic peak with a small OH contribution. Fig. 11 presents the XPS O 1s peak for 1000 L (saturation) H_2O exposure, at various temperatures, together with the (calculated from two Gaussian fits) ratio of OH to oxidic peak intensities for each temperature, showing a clear temperature trend of reduction of the OH contribution with temperature increase.

4. Discussion

Some of the result discussed, are compared to the reactions with Zr metal, extensively presented in Ref. [24] and references therein.

4.1. O_2/Zr_2Fe

O(DR) vs. exposure, for the various temperatures (Fig. 1), exhibits a clear temperature dependent behavior. Two distinct groups can be observed 300 K up to 620 K, where the saturation of O(DR) is achieved at about 10 L exposure (~20 L for 620 K) and the other group, 660–770 K, where the saturation is achieved at an order of magnitude of higher exposure and a ~20% lower value of intensity. Comparison to the AES adsorption/oxidation curves (Fig. 4) clarifies the processes, taking place on the surface. Here, the 300 K curve saturates at ~20 L exposure. Two additional groups can be observed 370–620 K where quasi-saturation is achieved and 670 K and up, where even at 1000 L exposure, no saturation is apparent.

Taking into account that DRS is sensitive only to the uppermost layer and AES monitors also the subsurface, a distinct difference between them points to strong inward diffusion. It seems that temperature dependent diffusion of oxygen to the subsurface and into the bulk, plays a critical role in forming the surface layer of adsorbed oxygen, oxide and dissolved oxygen. At room temperature, the similarity between the DRS and AES curves points to slow diffusion and slow buildup of a thin (significantly below AES detection range) oxide, also explaining the total low intensity of the oxygen AES signal, compared to higher temperature. Temperature enhanced oxygen dissolution and diffusion vacates surface adsorption sites on one hand and increases subsurface oxygen concentration. These two processes dictate different saturation values for O(DR) and O(AES). An increase in the inward diffusion of oxygen (Fig. 7), causes the jump down in the O(DR) saturation value as well as its rate of increase between 620 and 660 K (Fig. 1).

The nature of the alloy component that is oxidized is clear from the AES and XPS spectra (Figs. 2, 3, 5 and 6). Fig. 3 demonstrates that while Zr(metal) + Zr(oxide) stays about constant there is no Fe(oxide) component, observable in the AES spectra (Fig. 2) and the Fe(metal) peak decreases strongly with exposure to oxygen. The O/Zr(ox) curve, presented in Fig. 3 shows an initial higher value than for higher exposures, due to the presence of initially adsorbed oxygen [25,26], before oxidation starts (so it is not manifested in Zr(ox)). The saturation value, around 1.2 has no actual meaning (since both Zr(ox) and O were normalized differently) and its only significance is in the comparison to the value for H_2O/Zr, discussed in Section 4.2. The XPS spectra, in accordance, present Zr oxidation (Fig. 5), while Fe stays metallic (Fig. 6), but significantly decreases in intensity, in accordance with Fig. 2. The meaning is that the outer layer of the bulk is mainly composed of ZrO_2, supposedly by preferential oxidation driven segregation, with a small amount of metallic iron. A similar mechanism was observed for Zr metal [27], where, for higher temperatures (>800 K) oxidation, migration of oxygen to the oxide–metal interface was measured (which is also the case for Zircaloy-4, for atmospheric pressures and thick oxides [28]), but for the lower temperature range and thin oxide (similar to the present case) an outward migration of Zr was measured. This oxidation is the cause of degradation of the getter when exposed to an oxidizing atmosphere.

Fig. 5 emphasizes the composed effect of adsorption and reaction on one hand and dissolution and diffusion on the other hand.

For 300 K, oxidation of the outer thin layer is quite extensive, due to efficient adsorption as presented in Fig. 1. Fig. 4, on the other hand, depicts a saturation O(AES) value which is quite low, compared to those of other temperatures (indicating a thin oxide layer). This is the reason why metallic Zr^0 lines are observed in the XPS spectrum at 300 K (Fig. 5). The 620 K spectrum presents an efficient combination of adsorption and oxidation on one hand (Fig. 1) and dissolution and inward diffusion on the other hand, oxidizing also the subsurface. Therefore, the oxidized layer approaches the monitoring depth of XPS.

Surprisingly enough, the Zr(XPS) spectrum for 1000 L O_2/Zr_2Fe, at 770 K, shows only a metallic contribution, similar to the clean metal, in what looks as a contrast to the O(DR) and O(AES) intensities in Figs. 1 and 4, respectively. The explanation of this combination is that at this elevated temperature, adsorption and dissociation occur (so DRS and AES measure some adsorbed oxygen), but probably the oxygen concentration is within the solubility range, so no oxide is formed in the temperature–pressure regime of the current experiments. This dissolution of oxide into the bulk, for high temperatures is in accordance with measurements performed on metallic Zr [29].

4.2. H_2O/Zr_2Fe

Similar to the case of O_2/Zr_2Fe, the RT adsorption/oxidation by exposure to H_2O depicts (Fig. 9) a drastic decrease of Fe at the surface, with exposure and preferential oxidation of Zr buildup. However, some differences, compared to the O_2/Zr_2Fe exposure, can be observed:

The processes of Fe depletion and Zr oxidation are significantly slower. Even taking into account that every O_2 molecule contributes two O atoms to the oxidation and H_2O only one, saturation of the O(AES) curve is achieved for O_2 exposure around 80 L, while for H_2O exposure, the O(AES) curve is not saturated up to ~500 L exposure (Fig. 10).

While for O_2/Zr_2Fe Zr(m) + Zr(ox) is about constant, for H_2O/Zr_2Fe the sum shows a sharp decrease of almost 20%, with exposure, slowly climbing to the initial value. This is independent of the Fe decrease, which is very similar for both cases (taking into account the different process rates), but is in correlation with the slower increase of O(AES). Also O/Zr(ox) goes through a similar (but shallower) minimum. Like for the O_2 exposure, its initial values are high, due to oxygen adsorption. Through the whole oxidation range presented, the O/Zr(ox) value is around 1, significantly lower that that for O_2/Zr_2Fe that is ~1.2. This may point to an oxygen depleted oxide, formed for H_2O exposure, compared to that of O_2 exposure.

4.3. Oxide thickness

The average thickness of the growing oxide layer can be determine from the intensity ratio of the AES clean and oxidized zirconium signals, using the equation [30]:

$$n = (\lambda \cos\theta) \ln\left(\frac{I_{ZrO}}{I_{Zr}} + 1\right)$$

where n is the oxide thickness. λ, the electrons inelastic mean free path, was calculated to be ~0.6 nm for 150 eV kinetic energy, using the NIST database program [31]. $\theta = 42^\circ$ is the collecting angle of the cylindrical mirror analyzer. The oxidic (I_{ZrO}) and metallic (I_{Zr}) components of the AES spectra were calculated as described earlier and depicted in Fig. 3.

Oxide thickness vs. exposure for both O_2/Zr_2Fe and H_2O/Zr_2Fe at RT is presented in Fig. 12. Also presented is the oxide thickness of O_2 exposure vs. the atom dose (i.e. twice the exposure dose). It is clear that per reacted atom, the initial oxidation rate is similar for both gases, but while for O_2 exposure, saturation is achieved

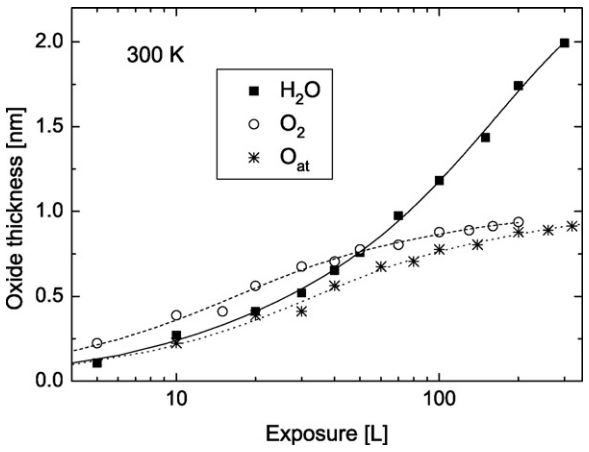

Fig. 12. RT oxide thickness vs. exposure to O_2 and to H_2O. The oxide thickness vs. oxygen exposure is also plotted for twice the dose, indicating a similar per O atom initial oxidation rate for both gases.

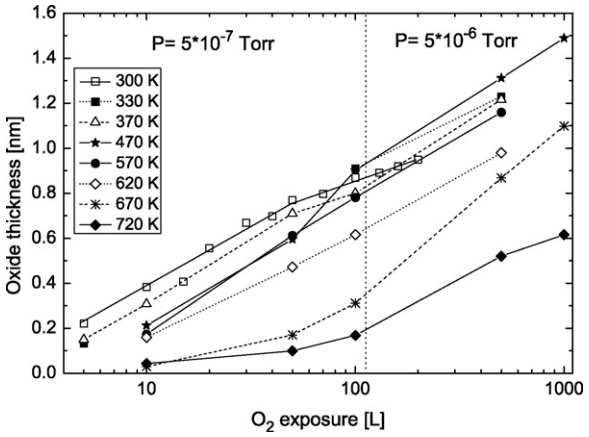

Fig. 13. Oxide thickness vs. exposure to O_2 at various temperatures. The pressure of oxygen at each exposure range is indicated.

at ~0.8 nm (about two unit cell average thickness [32]), for H_2O, at 2 nm thickness (for 300 L exposure), it is still increasing. The water formed oxide is depleted in oxygen by ~20% more than that formed by oxygen exposure (O/Zr(ox) for water exposure – Fig. 9 vs. that for oxygen exposure – Fig. 3). A possible explanation for this difference may be that dissolved hydrogen, originating from water dissociation, in the oxide, induces vacancies in it [33]. These oxygen vacancies may serve as preferred diffusion channels, thus enabling further oxidation. Also, incorporation of OH groups into the forming oxide (Fig. 11) might serve this enhanced oxidation, due to enhanced diffusion. A similar effect of enhanced diffusion due to formation of hydroxide on the surface was measured for water oxidation (vs. oxygen oxidation) of Zircaloy-4 [28].

Fig. 13 presents the oxide thickness, as a function of O_2 exposure, calculated for the various temperatures of the experiment. The growth also seems to be relatively pressure independent, in this temperature range, up to 620 K. Above 620 K, the dissolution of oxygen and its inward diffusion increases significantly (see Fig. 7) and higher oxygen pressure is needed to replace the oxygen diminishing from the surface. This is clearly manifested in the increase in the oxidation rate for 670 and 720 K, when the pressure is increased from 5×10^{-7} to 5×10^{-6} Torr.

The temperature–pressure dependence of the oxide thickness, formed on the surface, is also depicted in the comparison between AES (Fig. 13) and XPS (Fig. 5) results. The AES measurement shows that for up to 5×10^{-6} Torr the thickest oxide is formed at ~470 K.

Increasing the oxygen pressure to 1×10^{-5} Torr, increases the efficient oxidation temperature, as can be seen from the XPS results, where at 620 K a high flux of impinging O_2 molecules compensates the strong dissolution and inward diffusion of oxygen ions, the oxide thickness seems to be about the XPS probing depth.

Fig. 8 presents the O(DR) and H(DR) intensities vs. exposure to water vapor at various temperatures. Up to 370 K, the O(DR) curves are similar to each other. The H(DR) curves for this temperature range decreases between ~2 and ~5 L exposure, probably due to increased shadowing of H by O, associated with complete dissociation of the water molecules [21,23], in accordance with the O(DR) saturation. Above 5 L exposure, it increases, due to partial dissociation on top of the forming oxide and adsorption of hydroxyl groups on it, the hydrogen atoms of which are not shadowed. For 470 K, there is almost no hydrogen left on the surface and the little that stays (due to full dissociation of the water molecules) is mostly shadowed. The decrease of OH adsorption on the forming oxide with temperature increase is in accordance with the XPS O 1s spectra (Fig. 11), in which the OH portion of the intensity goes down from ~23% at 300 K, up to ~5% (which is in the error range and probably not existing, since H(DR) is not observed by DRS) at 770 K.

For 620 K and above, there is no hydrogen detected on the surface, probably due to no sticking and desorption of OH. Lower sticking, also for oxygen, together with inward enhanced diffusion, are probably the causes for the slower increase of O(DR) at 620 K. At 770 K, it levels out at >3 L exposure, at a much lower intensity than for the lower temperatures, due to the much increased inward diffusion. In contrast to the DRS saturation intensities for O(DR), the intensity of the XPS O 1s, at the various temperatures, is affected by the inward diffusion (monitoring a couple of nanometers), so, like for O_2 exposure, that of 620 K (and 1×10^{-5} Torr) is the highest (Fig. 11), having the optimum of sticking and diffusion combination. For the 300–470 K cases, that have similar adsorption curves, lower inner diffusion rate causes an integral lower intensity. This is in accordance with the fully oxidized Zr spectrum (not shown), while for 300 and 770 K, they are hardly oxidized similar to the O_2/Zr_2Fe behavior. Here too, it seems that for 770 K, oxygen is only adsorbed and absorbed (dissolved), rather than forming an oxide. This is in accordance with the fact that oxygen is highly soluble in zirconium, according to the Zr–O phase diagram [34]. Similar temperature effects were also found by Zhang and Norton [29] and Lyapin et al. [35] for the oxidation of zirconium metal in oxygen.

5. Conclusions

The surface of metallic Zr_2Fe was exposed to both oxygen and water vapor in order to study the effects of these gases, being the main degradation agents in its operation as a getter for hydrogen.

It was found that both gases oxidize the Zr component of the alloy, leaving the Fe component metallic and strongly diluted. Since Zr is the active component in the getter, the degradation effect is clear. For various temperatures, the oxidation is different. For O_2 at room temperature, the adsorption and dissociation are efficient, leading to fast oxidation on the surface, forming a thin oxide layer (~0.8 nm pseudo-saturation for oxygen, in the 300 L exposure range), not penetrating much into the bulk. At 620 K, which is the operating temperature of the getter, the oxidation is most effective, since both the adsorption and inward diffusion are efficient enough, so XPS monitors a full oxidized layer (~5 nm). For the 770 K exposure, the growing oxide is predominated by extensive dissolution of the oxygen into the substrate, leaving an oxygen depleted layer (probably solid solution) on the surface, as depicted by all 3 techniques.

The initial sticking coefficient per oxygen atom, at RT, is similar for oxygen and water vapor, but the oxide thickness for H_2O is more than twice of that for O_2, which points to a different oxidation mechanism. The difference may be due to the lower oxygen concentration for H_2O/Zr_2Fe, forming vacancies that are diffusion routs or incorporation of hydrogen or hydroxyl groups in the oxide layer, thus enabling further inward growth. For the low temperature regime (non operation period), H_2O is a more effective contaminant in degradation of the getter.

Acknowledgements

The authors would like to thank Y. Zeiri and D. Cohen for initiating the study and for helpful discussions and E. Tiferet for his help in performing the experiments.

References

[1] A.E. Proromides, C. Scheuerlein, M. Taborelli, Appl. Surf. Sci. 191 (2002) 300.
[2] P. Manini, A. Bonucci, A. Conte, S. Raimondi, Proc. EPAC, Edinburg, Scotland, 2006.
[3] Y. Suestugu, K. Shibata, M. Shira, Nucl. Instrum. Methods Phys. Res. A 597 (2008) 153.
[4] M. Colman, D. Chandra, J. Werner, T.J. Udovic, in: D. Chandra, R.G. Bautista, L. Schlapbach (Eds.), Advanced Materials For Energy Conversion II, TMS, 2004.
[5] S. Fukada, Y. Toyoshima, M. Nishikawa, Fusion Eng. Des. 49–50 (2000) 805–809.
[6] S. Fukada, K. Tolamaga, M. Nishikaw, Fusion Eng. Des. 36 (1997) 471.
[7] J. Kovac, O. Sakho, P. Manini, M. Sancrotti, J. Vac. Sci. Technol. A 18 (2000) 2950.
[8] K.J. Maynard, N.P. Kherani, W.T. Shmayda, Fusion Technol. 28 (1995) 1546.
[9] W.T. Shmayda, N.P. Kherani, A.G. Heics, J. Vac. Sci. Technol. A 6 (1998) 1259.
[10] F. Aubertin, U. Gonser, S.J. Campbell, J. Less-Common Met. 101 (1984) 437.
[11] C. Boffito, F. Doni, L. Rosi, J. Less-Common Met. 104 (1984) 149.
[12] H. Masanori, R. Hayakawa, Y. Kaneko, K. Watanabe, J. Alloys Compd. 352 (2003) 218.
[13] J. Kovac, O. Sakho, P. Manini, M. Sancrotti, Surf. Interface Anal. 22 (2004) 327.
[14] P. Manini, M. Sancrotti, G. Trezzi, J. Vac. Sci. Technol. A 9 (1991) 182.
[15] A. Bastianon, L. Braicovich, B. De Michelis, Surf. Sci. 264 (1992) 423.
[16] E. Puppin, L. Braicovich, B. De Michelis, P. Vavassori, E. Vescovo, Surf. Sci. 264 (1992) 429.
[17] M.H. Mintz, U. Azmony, N. Shamir, Surf. Sci. 185 (1987) 413.
[18] J.W. Rabalais, CRC Crit. Rev. Solid State Mater. Sci. 14 (1988) 318.
[19] M.S. Hammond, J.A. Schultz, A.R. Krauss, J. Vac. Sci. Technol. A13 (1995) 1136.
[20] M.H. Mintz, J.A. Schultz, J. Less-Common Met. 103 (1984) 349.
[21] M.H. Mintz, N. Shamir, Appl. Surf. Sci. 252 (2005) 633.
[22] N. Shamir, E. Tiferet, S. Zalkind, M.H. Mintz, Surf. Sci. 600 (2006) 657.
[23] Y. Nishimo, A.R. Krauss, Y. Lin, D.M. Gruen, J. Nucl. Mater. 228 (1996) 346.
[24] N. Stojilovic, E.T. Bender, R.D. Ramsier, Prog. Surf. Sci. 78 (2005) 101.
[25] S. Zalkind, M. Polak, N. Shamir, Surf. Sci. 513 (2002) 501.
[26] S. Zalkind, M. Polak, N. Shamir, Surf. Sci. 601 (2007) 1326.
[27] L.P.H. Jeurgens, A. Lyapin, E.J. Mittemeijer, Acta Mater. 53 (2005) 4871.
[28] A. Grandjean, Y. Serruys, J. Nucl. Mater. 273 (1999) 111.
[29] C. Zhang, P.R. Norton, J. Nucl. Mater. 300 (2002) 7.
[30] J.F. Watts, J. Wolstenholme, An Introduction to Surface Analysis by XPS and AES, Wiley, 2003.
[31] C.J. Powell, A. Jablonski, NIST Electron Inelastic-Mean-Free-Path Database – Version 1.1, National Institute of Standards and Technology, Gaithersburg, MD, 2000.
[32] A.T. Heuer, M. Rühle, Advances in Ceramics, The American Ceramics Society, 1984.
[33] Y. Fukai, N. Okuma, Phys. Rev. Lett. 73 (1994) 1640.
[34] IAEA-TECDOC-996, Viena, 1998, p. 27.
[35] A. Lyapin, L.P.H. Jeurgens, E.J. Mittemeijer, Acta Mater. 53 (2005) 2925.